Reynolds stress statistics in the near nozzle region of coaxial swirling jets

Viacheslav Stetsyuk

School of Computing and Engineering,
University of Huddersfield, UK
Email: v.stetsyuk@hud.ac.uk

John Chai Chee Kiong

School of Computing and Engineering,
University of Huddersfield, UK
Email: J.Chai@hud.ac.uk

Abstract: Particle image velocimetry (PIV) was used to obtain the mean axial velocity u, the mean radial velocity v and the Reynolds stress statistics in an isothermal flow formed by discharging a central jet in an annular stream of swirling air flow. This is a typical geometry used in swirl-stabilised burners, where the central jet is the fuel. The flow Reynolds number was 29000, based on the area-averaged velocity of 8.46 m/s at the exit and the diameter of swirling co-flow of 50.8 mm. Three swirl numbers, *S*, of 0.3, 0.58, and 1.07 of the annular swirling stream were considered. The effects of the swirl number on the behaviours of the Reynolds stresses, and their gradients, which appear in the Reynolds-averaged Navier-Stokes (RANS) equations are analysed. The results show pronounced asymmetry in the mean and the fluctuating quantities for all swirl numbers. The flow asymmetricity is found to be related to the radial velocity fluctuations. The ratio of $\overline{u'^2}/\overline{v'^2}$ was found to be circa 0.5 and was independent of the flow swirl number. The values of $\overline{u'v'}$ were circa 5-10% of $\overline{v'^2}$. It was postulated that for swirling flows with constant Reynolds number the change in the flow swirl number only, does not necessary result in increase of turbulent intensity. An 'effective' turbulent viscosity was shown to be independent of the flow swirl number for constant Reynolds number.

Keywords: Reynolds stress, swirling jet, RANS, coaxial

Reference to this paper should be made as follows: Stetsyuk & Chai (2018) 'Reynolds stress statistics in the near nozzle region of coaxial swirling jets', *Int. J. Hydromechatronics*, Vol. X, No. Y, pp.000–000.

Biographical notes: Viacheslav Stetsyuk is currently a Lecturer in Engine Systems at the Department of Engineering and Technology of the School of Computing and Engineering, University of Huddersfield, UK. He received his MSc from the Technion-Israel Institute of Technology and a PhD from Imperial College London in the research area of experimental fluid dynamics. His research interests include experimental fluid dynamics, signal processing and non-intrusive diagnostic techniques.

John Chai is currently a Professor at the Department of Engineering and Technology of the School of Computing and Engineering, University of Huddersfield, UK. He is an Adjunct Professor of Xian Jiaotong University, Shanxi, China and Chinese University of Petroleum – East China, Qingdao, Shandong, China. He is an elected Fellow of ASME. He received his MSc from the University of Wisconsin-Milwaukee and a PhD from University of Minnesota in the research area of numerical heat transfer. His research interests include the development of numerical techniques for complex multiphysics transport phenomena encountered in multi-phase flows and fluid-structure interactions. He has published over 80 journal articles, over 90 conference articles and contributed a chapter to the second edition of the Handbook of Numerical Heat Transfer.

1 Introduction

Flows with swirl can be found in a large number of industrial applications, e.g. in swirl-stabilised burners (Lilley, 1977), gas cyclone separators (Hoekstra *et al.*, 1999), jet pumps and ejectors (Ribeiro & Whitelaw, 1980). In flows with swirl, the tangential velocity component

creates pressure gradients (Farokhi *et al*., 1992) leading to the formation of low pressure regions within the central core of the swirling jets. At a certain degree of swirl, the momentum of the rotating fluid can no longer overcome the adverse pressure gradient created by the swirling motion. This results in flow reversal and vortex breakdown (Gupta, 1985), which enhances turbulent mixing and acts as the source of constant ignition (Lilley, 1977; Syred & Beer, 1974) in, e.g. industrial burners and gas-turbine combustors. The effect of swirl on turbulent jets is, therefore, of fundamental importance and much practical relevance. In this work, the swirl number was defined as by Gupta et al. (2009).

$$S = \frac{2G_\theta}{G_x D} \qquad (1)$$
$$G_\theta = 2\pi\rho \int_{r=r_i}^{R} WrUdr$$
$$G_x = 2\pi\rho \int_{r=r_i}^{R} UUrdr$$

where the parameters of the above and all the following equations are defined in Section 6 of the paper.

Experimental work on swirling coaxial jets can be dated back to the 1962 when measurements of the mean velocity components and one of the Reynolds stresses in a swirling turbulent round jet emerged from a rotating pipe were presented (Rose, 1962). Other initial works were dedicated to the measurements of the mean velocities and the static pressure by using hot-wire anemometry and five-hole impact probes (Ribeiro & Whitelaw, 1980; Craya & Darrigol, 1967; Chigier & Beer, 1964).

Despite of its importance, studies of swirling flows were generally limited to low and intermediate swirl numbers, e.g. Ribeiro & Whitelaw, 1980 (*S*=0.26); Facciolo, 2006 (*S*=0-0.5); Orlu, 2006 (*S*=0-0.5); Toh, 2005 (*S*=0.06-0.15), Gilchrist & Naughton, 2005 (*S*=0-0.23); Oljaca *et al*., 1998 (*S*=0-0.24), Feyedelem & Sarpkaya, 1998 (*S*=0-0.52); Park & Shin, 1993 (S=0-1.87); Milosavljevic, 1993 (*S*=0.3, 0.58, 1.07); Mehta et al., 1991 (*S*=0-0.2); Farokhi, 1989 (*S*=0.48); Elsner & Kurzak, 1989 (*S*=0-0.42); Samet & Einav, 1988 (*S*=0-0.49).

Several swirl generators were used, e.g. rotating pipe was used as swirl generator in the work of Facciolo (2006) and Orlu (2006), while tangential injection was used in the present work and in the work of Ribeiro & Whitelaw (1980); Toh (2005), Gilchrist & Naughton (2005); Feyedelem & Sarpkaya (1998), Milosavljevic (1993); Farokhi (1989) and Samet & Einav (1988). Rotating paddle was used by Oljaca *et al*. (1998) and rotating honeycomb was used by Mehta *et al*. (1991). Finally, passive vanes were used in the work of Elsner & Kurzak (1989).

Technically speaking, different swirl generators should influence both the distribution of mean velocities and the Reynolds stresses and, therefore, can result in non-symmetric flow distribution. For example, tangential injection with milled slots or nozzles as well as passive vanes are not axisymmetric and, therefore, phase-dependent variations must arise in the ensemble mean velocities and the Reynolds stresses. However, rotating pipe is virtually axisymmetric if there are no alignment errors and, therefore, no phase-dependent variations must arise in the ensemble mean velocities and the Reynolds stresses.

Proper closures of the ensemble-averaged RANS equations are critical to the modelling of turbulent flows. In the RANS equations, the Reynolds decomposition and the associated ensemble averaging over some time, which can be an infinite time in an ergodic flow, are used. Upon substitution of the Reynolds decomposition with $u = U + u'$, $v = V + v'$, $w = W + w'$ and ensemble averaging, the Reynolds stress terms appear as unclosed quantities in the momentum equations. There are six independent Reynolds stress terms, three tangential stress terms $\overline{u'v'}$, $\overline{u'w'}$, $\overline{v'w'}$ and three normal stress terms $\overline{u'^2}$, $\overline{v'^2}$, $\overline{w'^2}$ that must be modelled.

The previously available information on turbulence structures of coaxial jets with low to high swirl numbers still does not provide a thorough understanding of the transport process in these flows. No spatial distributions of the Reynolds stresses as a function of swirl number have been studied in detail, which is of primary importance. The major objective of the present work is to obtain measurements, in coaxial jet flows with different degree of swirl, that will improve understanding of the unknown quantities in the RANS equations.

The remainder of this article is structured as follows. The next section II describes the experimental arrangement and atmospheric burner, which was used to generate swirling jets with different degrees of swirl. Subsequent section III discusses the spatial distributions of the mean velocity, the standard deviation of the velocity fluctuations, the Reynolds stress components. The Schwarz inequality is also presented for completeness. The article ends with a summary of the main conclusions.

2 Experimental apparatus and procedure

The flow section (Fig. 1) consisted of two concentric pipes with the annulus section supplying swirling air and the central pipe delivering non-swirling air jet. The central pipe (non-swirling) has an inner diameter D_f of 15 mm and an outer diameter of 18 mm. The inner diameter of the outer pipe delivering swirling co-flow *D* was 50.8 mm.

The inner pipe is centred within the outer pipe by three screws at 25 mm upstream of the burner exit. The flow development section was 264 mm long to minimise the phase-dependent variations in the ensemble mean velocities and the Reynolds stress due to the non-axisymmetric swirl generator.

The traversing mechanism was built from a surface grinding and milling machine table. The flow section was firmly attached to the table. The table allowed displacement in one direction (axial) only with an accuracy of 0.5 mm. No radial displacements were allowed.

The non-swirling central jet Reynolds number based on the area-averaged axial velocity of 3.77 m/s and the diameter D_f of 15 mm was 3770. The swirling flow

Reynolds number based on the area-averaged velocity of 8.46 m/s at the exit and the diameter of annular swirling stream D of 50.8 mm was 29000.

The swirling stream was created by passing air through a static swirler containing six milled tangential slots to impart angular momentum. The static swirler was located in a plenum chamber in which the swirling air was combined with the second stream that delivered 'axial air'. Metal plates were installed in the axial and tangential air sections of the plenum chamber to ensure that the axial and tangential air streams were distributed uniformly upstream of the inlets into the annular air supply stream, where they were combined to control the strength of the swirl at the exit.

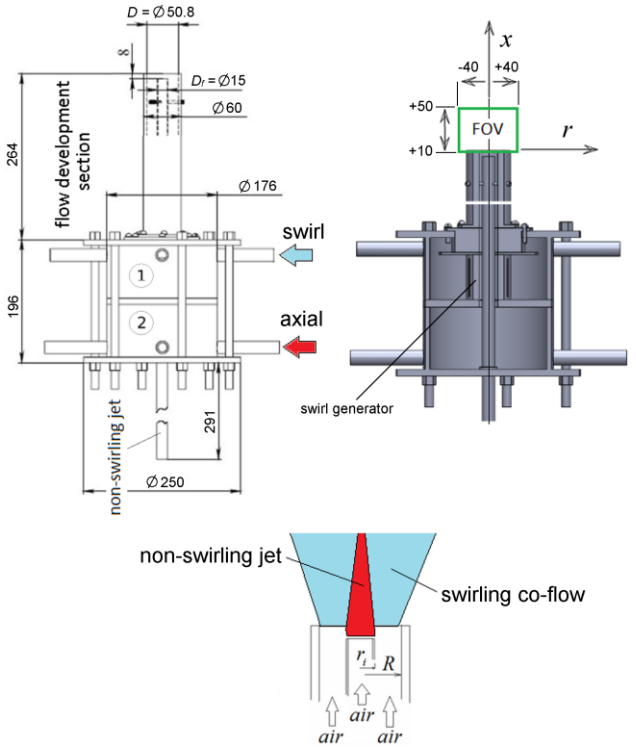

Figure 1: Experimental configuration and arrangement of coaxial jets. Field of view is shown as 'FOV'. All dimensions are in mm.

The axial direction, parallel to the flow propagation and radial direction perpendicular to the axial direction are denoted as *x* and *r*. The swirl number used as the primary variable was computed by using the velocity profiles initially obtained by Laser Doppler Anemometry, Milosavljevic (1993).

During experiments the air referred to as the swirling component was measured by a KDG Rotameter Series 2000 variable-area flowmeter, which was individually calibrated to accuracy of Class 1.6 (VDI/VDE3513), i.e. ±1.2% of indicated flow and ±0.4% full scale reading. The axial component of air was measured by Fisher Control Limited flowmeter rated at a maximum flow of 1000 l/min and was also calibrated to accuracy of Class 1.6 (VDI/VDE3513).

Systematic uncertainty of the swirl numbers was computed as 0.3±0.0152, 0.58±0.0288 and 1.07±0.0657. Uncertainty in Reynolds number was computed as 28662±1456 (S =0.3), ±1422 (S =0.58) and ±1760 (S =1.07). Finally, uncertainty in bulk velocity of swirling co-ow for S = 0:3; 0:58 and 1.07 was computed as 8.46±0.430, ±0.420 and ±0.519 m/s.

The PIV system consisted of a frequency-doubled (532 nm) dual-pulsed Nd:YAG laser (item 5 in Fig. 2) from Litron Lasers Ltd and a double-frame

CCD camera (item 6 in Fig. 2). The sheet forming optics consisted of two mirrors (items 1 and 4 in Fig. 2) a plano-concave (item 2 in Fig. 2) with focal length of -20 mm, a plano-convex (item 3 in Fig. 2) with focal length of 200 mm and a cylindrical positive lens (item 10 in Fig. 2) with focal length of 310 mm. The sheet forming optics formed a laser sheet of 50 mm width and the final positive lens was used to focus the laser beam into a thin waist, with focal point located at the axis of symmetry of the flow. The average laser energy at the exit port of the laser was circa 20 mJ/pulse. The thickness of the laser sheet was measured and found to be 0.5 mm at $1/e^2$ of the Gaussian intensity distribution. Perspective distortion was corrected by using a three-dimensional imaging target.

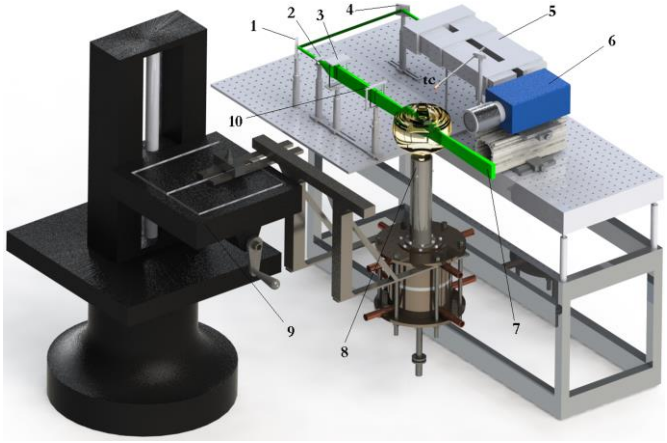

Figure 2: A 3D model of an optical arrangement used in particle image velocimetry.

A double frame CCD camera from LaVision Inc. (Imager Intense) was used in this work. The camera was equipped with a Nikon lens with focal length of 50 mm and aperture of 1.2. A 13 mm extension ring was also used after the camera lens for closer focusing. A 532-3 bandpass filter was used in the front of the camera lens in order to block any incoming ambient light and unwanted reflections that might interfere with the acquired signal, thus transmitting only wavelength of 532±1.5 nm. The camera exposure time was set to 1 μm at the maximum aperture of 1.2. The synchronisation of the laser flash-lamp and the CCD camera was performed by using a programmable PC-based timing unit using TTL pulses.

PIV is based on two subsequent recordings with a short time delay between them. Derivation of velocity vectors is performed by a cross-correlation of a pair of interrogation windows from two exposed recordings. The cross-correlation procedure is repeated for each interrogation window over the two images captured by the camera, producing a signal peak in each interrogation window. A sub-pixel interpolation is used to measure the velocity with higher accuracy. In this research, the separation time

between two PIV frames was 60 μs. A multi-step cross-correlation algorithm was used with an initial interrogation window of 64×64 pixels and resulting interrogation window of 32×32 pixels. This corresponded to a spatial resolution of 2 mm and velocity vector spacing of 1 mm. In terms of Batchelor length scale the corresponding spatial resolution is $6\lambda_\beta$ and velocity vector spacing is $2.5\lambda_\beta$. The Batchelor length scale λ_β was in the range of 300-400 μm for the range of S of 0.3-1.07 and was computed from the dissipation rate spectra at the wavenumber corresponding to 2% of the peak value of the dissipation rate spectrum (Stetsyuk *et al.*, 2016).

The swirling air co-flow and central non-swirling jet were seeded with Aluminium oxide Al_2O_3 particles with a diameter of 1 μm Velocity was computed from particle Mie scattering intensity images by using a commercial PIV software provided by LaVision Inc. (DaVis 7.2). Since, the velocity computation is directly dependent on a number of particles in the flow, it is advised to have at least 10 to 20 particles per interrogation window. The three-point Gaussian peak fit was used as a sub-pixel estimator Stanisla *at al.* (2005).

The accuracy of the measurements is dependent on the ability of the particles to follow the flow and adjust their velocity to the flow fluctuations. If the flow is subjected to extreme acceleration, the inertia of the particles can affect the velocity measurements and all the Reynolds stresses. The particle response to turbulent fluctuations is characterised by the Stokes number, which is the ratio of the stopping distance of a particle to a characteristic dimension of the obstacle. Velocity tracing accuracy errors for particles with the Stokes number <<1 are below 1% (Tropea *et al.*, 2007). Aluminium oxide particle response has the smallest Stokes number compared with other seeding options.

3 Results and discussions

The spatial distributions of the mean velocity, the vorticity and the standard deviation of the velocity fluctuations are presented and discussed in this section. An important parameter in the study of turbulence namely, the vorticity is presented for completeness. The vorticity ω can be seen as the instantaneous rigid body-like vortex of fluid particles rotating at a given angular rate without shear deformation, i.e. without relative velocity between adjacent fluid particles. It is defined as twice the instantaneous rigid body rotation rate of the fluid particles defined by the curl of the velocity field (Panton, 2013). In this work, the vorticity at a point *x*, *r* was computed from the mean axial *u* and the mean radial *v* velocity components.

$$\omega = \frac{\partial v}{\partial x} - \frac{\partial u}{\partial r} \tag{2}$$

The velocity magnitudes were computed from 1000 instantaneous PIV images acquired at 2.5 Hz with a time averaging window of 400 s. In order to validate the temporal assumption (converged averages), the mean velocities and the variances were also computed using 1000 and 5000 PIV images. It was found that the temporal assumption was plausible for all swirl numbers, as the mean and the variance were constant for the two sets of images. Therefore, 1000 images were only kept to minimise storage requirements.

Figure 3 shows the spatial distributions of the measured mean velocities coloured by the velocity magnitudes and by the vorticities. The vorticities were computed from the mean velocity spatial distributions shown in the same figure. The position of the edges of the central pipe delivering the non-swirling jet is shown by the short thick red lines at $r\approx\pm8$ mm. The position of edges of the annulus supplying swirling air is shown by the thin green lines at $r\approx\pm25$ mm. The top row corresponds to the lowest swirl number of 0.3 and the bottom row is S=1.07.

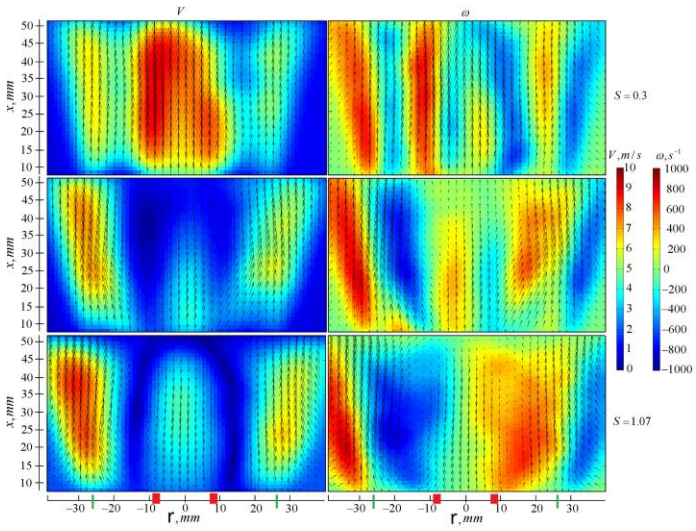

Figure 3: Measured spatial distribution of mean velocity magnitude (left) and mean velocity vector field coloured by the vorticity (right) as a function of flow swirl number. The position of the edges of the central pipe delivering the non-swirling jet is shown by the short thick red lines at r≈±8 mm. The position of edges of the annulus supplying swirling air is shown by the thin green lines at r≈±25 mm. From top to bottom S=0.3, 0.58 and 1.07

The flow exhibits a jet-like structure for S=0.3, which is expected at such a low flow swirl number. The velocities along the centreline jet remains nearly constant with pronounced asymmetry on the right-hand side. The entrainment of ambient air is seen and persists up to 50 mm from the burner exit. Vorticity, which can be seen as the local angular rate of rotation, in the case of low swirl number is solely linked to the effects of shear stress and hence, can be termed as shear vorticity. As expected, the maximum vorticity is expected to be within the confines of the central pipe, i.e. $r\approx\pm10$ mm and within the regions of air entrainment, i.e. $r\approx\pm30$.

Surprisingly, the spatial distributions of the vorticity are not axisymmetric. It can potentially be linked to the non-axisymmetric swirl generator with its 6 tangential slots. However, the flow development section is relatively long and, therefore, one can expect that the effects of non-axisymmetric swirl generation are minimised and there should be no variations in the spatial distributions of the mean velocities and the mean vorticity about the jet axis.

Qualitatively different picture is observed when the swirl number increases to 0.58. At this swirl number, the flow reversal and vortex breakdown leading to the formation of the recirculation zone is expected (Gupta, 1985). Even though, no fully recirculation zone is seen (Fig. 5) middle row), its presents can be detected by the rapid deceleration of the centreline velocity within the confines of the non-swirling jet. Unlike pure swirling flows (without central jets), the weak recirculating flow created by the outer swirling jet cannot overcome the axial momentum of the inner jet. As a result, no pronounced recirculating flow is observed at S=0.58. However, this weak recirculation zone acts as an aerodynamic blockage, which reduces the centreline velocities and creates isolated stagnation zone at $r\approx$-15 mm and 30<x<45 mm. Therefore, it is postulated that the extent of the recirculation zone is dependent on the momentum ratio between the central non-swirling and the co-flowing swirling jets. Depending on the momentum ratio, both fully and partially developed recirculation zone can be observed at S=0.58. The maximum value of vorticity magnitude for S=0.58 is similar to that found for S=0.3 but with higher eccentricity.

Unlike the intermediate swirl number, the recirculation zone is fully developed and clearly seen for S=1.07. Extended internal recirculation zone is formed as a result of strong back flow that collides with the central non-swirling jet. Since the momentum of the reverse flow is higher than the central jet, as a result, a well-defined recirculation zone is formed. The flow shape resembles that of a tulip and is almost symmetrical.

It has also been suggested that swirling flows in pipes usually had some levels of asymmetricity (Kito, 1984). Small deviations of velocity distributions in the flow development section can cause non-negligible asymmetricity at downstream locations, which can also be enhanced by the with non-axisymmetric swirl. It was also suggested by Kito (1984) that the eccentricity of swirl can be amplified downstream only for a certain range of flow swirl numbers, which is also confirmed by the present study, i.e. the flow asymmetricity is higher for low swirl number.

Large values of vorticity are found localised at the shear layer between the non-rotating axial jet and the swirling co-flow for all swirl numbers. Positive and negative values of vorticity indicate local velocity vectors in opposite directions. It is important to note that flow asymmetricity induces corresponding asymmetricity in all linked variables, i.e. scalar and temperature. It has been independently confirmed by the measurements of passive scalar spatial distributions using the same operating conditions (Stetsyuk *et al*., 2016).

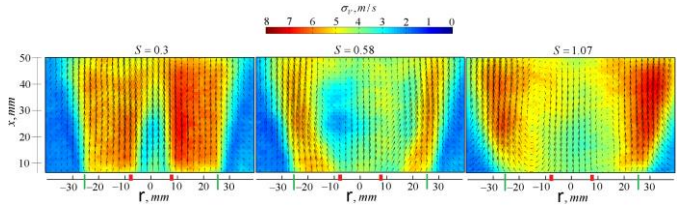

Figure 4: Measured standard deviation of velocity fluctuations for annular flow swirl number of 0.3, 0.58, and 1.07.

Figure 4 shows the measured standard deviations of the velocity fluctuations superimpose on the mean velocity vectors. The standard deviations of velocity fluctuations were computed as follows:

$$\sigma_V = \sqrt{\frac{1}{N}\sum_{i=1}^{N}\left(V-\overline{V}\right)^2} \tag{3}$$

The velocity magnitudes V were computed as.

$$\overline{V} = \frac{1}{N}\sum_{i=1}^{N}\sqrt{u^2+v^2} \tag{4}$$

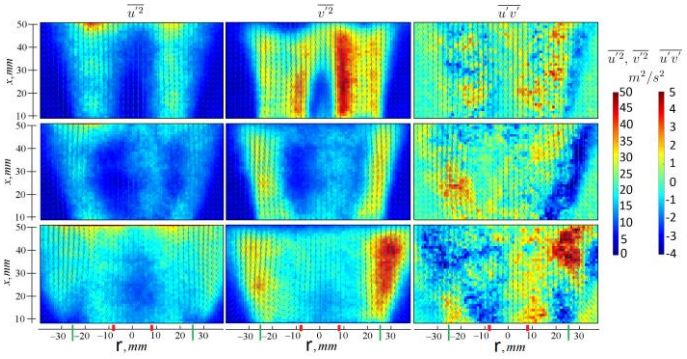

Figure 5: Spatial distribution of the Reynolds stresses as a function of flow swirl number. From top to bottom: S=0.3, 0.58 and 1.07. Note that $\overline{u'^2}$ is the Reynolds stress component in x direction and $\overline{v'^2}$ is along r direction. Scale 0-50 corresponds to $\overline{u'^2}$ and $\overline{v'^2}$, while scale -4-5 corresponds to $\overline{u'v'}$. Note that the mean velocity vectors are superimposed on the Reynolds stresses.

Due to these limitations, the orientation of velocity fluctuation vectors may be away from the plane of the measurements. When this happens, $\overline{u'^2}$ and $\overline{v'^2}$ do not fully represent fluctuations along the measurement plane, which lies in the x and r directions. It can be assumed that at the low swirl number, the velocity component perpendicular to the measurement plane is negligible. In this situation, the measurements can be considered as the 'true' statistics of the velocity fluctuations in the x and r directions. However, in the absence of full 3D measurements of the Reynolds statistics from the burner discussed in this article, surrogate statistics obtained from two-dimensional measurements are valuable in the understanding of fundamental physics. However, direct extrapolation of the presented results to other swirling flows should been done with care.

The non-swirling central jet exhibits constant and relatively low standard deviations of the velocity fluctuations, which are around 3 m/s up to $x/D_f \approx 2$ and then almost linear increase of the standard deviation is observed for S=0.3. The annular swirling core, however, exhibits

higher standard deviations of the velocity fluctuations, which are circa two times more than the corresponding fluctuations in the non-swirling central jet. Different behaviours are observed at swirling flow at S=0.58 and 1.07. Rapid deceleration of the centreline velocities at S=0.58 leads to lower velocity fluctuations within the extended near burner zone. This process, we term as the damping effect of the recirculation zone. Somehow similar behaviour is also seen for S=1.07. Full recirculation zone was formed and up-flowing non-swirling jet reduces the velocity fluctuations of recirculating down-flowing stream.

In should be noted that the calculation of turbulent statistics involves the assumption of flow temporal stationarity. The flow stationarity means that the flow mean velocity and the velocity variance is independent of time or at least are constant during the time averaging process

A possible bias in the evaluation of the Reynolds stresses can be encountered in our analysis. This is because no whirl velocity component can be measured using typical planar measurements where the PIV camera is positioned perpendicular to the flow axial direction. In order to measure the swirl velocity component, a mirror, or a camera has to be positioned along the flow axial direction. This is difficult to achieve in practice due to physical constrains. Alternatively, a 3D PIV setup can be used, which also has its own drawbacks linked to the resolution of the 3rd velocity component.

From Figures 5 to 8, the maximum of $\overline{u'^2}$ was around 25 m^2/s^2, the maximum of $\overline{v'^2}$ was found to be circa 50 m^2/s^2, while the maximum of $\overline{u'v'}$ was 10 times smaller for all flow swirl numbers. $\overline{u'v'}$ is nearly isotropic for S=0.3. A nearly isotropic distribution of $\overline{u'^2}$ with values of circa 15 m^2/s^2 is found within the confines of the co-flowing swirling jet, while value of circa 1.5 m^2/s^2 was found within the confines of the non-rotating central jet for S=0.3 unlike for S=0.58 and 1.07. This nearly isotropic distribution was also confirmed by, e.g. Ribeiro & Whitelaw (1980) for similar swirl number of 0.26. The assymetry in $\overline{v'^2}$ and $\overline{u'v'}$ is clearly seen in Figures 5 to 8. However, the axial component $\overline{u'^2}$ is reasonably symmetric. Almost symmetrical shape of $\overline{u'^2}$ suggests that the fluctuations along the x direction are similar and spatially invariant and the flow asymmetry can be attributed to the fluctuations perpendicular to the jet axis.

The middle row in Figure 5 shows the spatial distributions of $\overline{u'^2}$, $\overline{v'^2}$ and $\overline{u'v'}$ for the flow swirl number of 0.58. As before, fluctuations along x directions are low and the values of $\overline{u'^2}$ are close to 15-20 m^2/s^2. Nearly zero values of $\overline{u'^2}$ are found within the confines of weak recirculation zone. The same trend is also observed for $\overline{v'^2}$. The maximum values of $\overline{v'^2}$ are found in the shear layer between still surrounding air and the swirling co-flow and are spread radially outwards. Compared to the flow swirl number of 0.3, lower values of $\overline{u'^2}$ are found at the interface between the ambient air entrainment and the swirling co-flowing jet (right side). The values of $\overline{u'v'}$ are within -4 to 5 m^2/s^2. Even though, the flow outside of the swirling co-flowing jet seems to be induced by the swirling co-flow, i.e. the surrounding air flows radially inward, which is clearly visible for all flow swirl numbers, the Reynolds stress components are nearly zero in regions outside the rotating co-flow.

The bottom row in Figure 5 shows spatial distributions of fluctuating quantities for the highest flow swirl number of 1.07. The maximum values of $\overline{u'^2}$ and $\overline{v'^2}$ are similar to those found in S=0.3. The spatial distribution is more symmetric and nearly isotropic. It was demonstrated, e.g. by Clayton & Morsi (1985) that the presence of swirl increases turbulence intensity. In this work, however, it was found that for all three swirl numbers, the magnitudes of the Reynolds stresses are similar, while the spatial distributions are different. We, therefore, postulate that for constant Reynolds number, change in the swirl number has very little influence on the turbulent intensity.

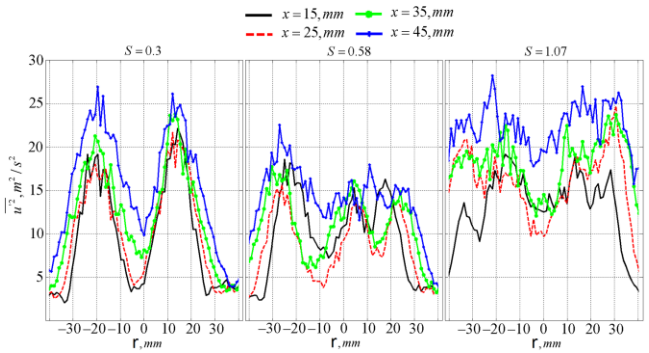

Figure 6: Radial profiles of $\overline{u'^2}$ Reynolds stress component as a function of flow swirl number at different axial locations. These profiles were extracted from Fig. 5.

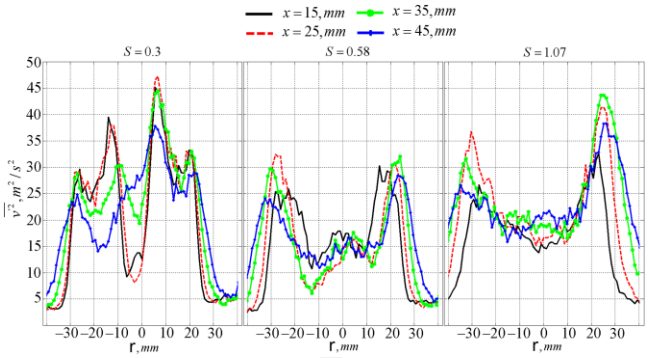

Figure 7: Radial profiles of $\overline{v'^2}$ Reynolds stress component as a function of flow swirl number at different axial locations. These profiles were extracted from Fig. 5.

This can be arrived at by examining the basic definition of the turbulent intensity, which is defined as $I \equiv U_{rms} / \sqrt{U^2 + V^2 + W^2}$, where U_{rms} is the room-mean-square (RMS) of the velocity fluctuations, U,V,W are the time-averaged axial, radial and tangential velocities. The RMS of velocity fluctuations are computed as $U_{rms} = \sqrt{\left(\overline{u'^2} + \overline{v'^2} + \overline{w'^2}\right)/3}$. Though $\overline{w'^2}$ were not measured, they are related to $\overline{u'^2}$ and $\overline{v'^2}$ via the continuity equation. As U,V,W, $\overline{u'^2}$, $\overline{v'^2}$ and $\overline{w'^2}$ (via the continuity equation) are

independent of the swirl number, the RMS of velocity fluctuation is also expected to be independent of the swirl number.

Quantitative behaviours of the Reynolds stress components are shown in Figures 6-8. These profiles were extracted from Figure 5 at four different axial positions, namely 15 mm, 25 mm, 35 mm and 45 mm downstream of the burner exit for three swirl numbers. For the smallest swirl number of 0.3, distinct regions are observed in the $\overline{u'^2}$ and $\overline{v'^2}$ profiles. The first is for x=15 mm and x=25 mm. In these regions the fluctuations are similar and smaller in values. This is likely due to the fluctuations in the core central non-swirling jet flow. The magnitudes of these fluctuations are larger at x=35 mm and x=45 mm. At these locations it is possible that the swirling annulus flow has mixed with the central non-swirling fluid. This mixing intensifies the fluctuations. The fluctuations in the annular region are almost the same in all four locations. The fluctuations for the two larger swirl numbers are almost the same for all four locations. This may imply that the swirling flow has already mixed with the central jet flow at these locations.

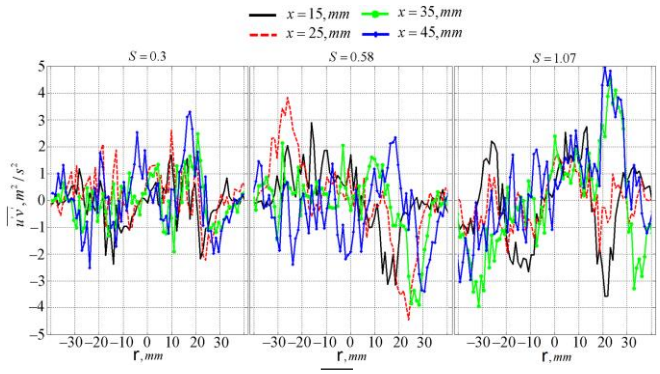

Figure 8: Radial profiles of $\overline{u'v'}$ Reynolds stress component as a function of flow swirl number at different axial locations. These profiles were extracted from Fig. 5.

Figure 9 also shows the source terms for the RANS equations. The raw form of the source terms due to the gradients of the Reynolds stresses and the source terms due to Boussinesq approximation based on the gradients of the mean velocities to close the Reynolds stress are shown. If an appropriate expression is found for eddy viscosity, then these source terms can be used to close the Reynolds stresses.

$$S_u = \frac{\partial}{\partial x}\left(\mu_t \frac{\partial \bar{u}}{\partial x}\right) + \frac{\partial}{\partial y}\left(\mu_t \frac{\partial \bar{v}}{\partial x}\right) \qquad (5)$$

$$S_v = \frac{\partial}{\partial x}\left(\mu_t \frac{\partial \bar{u}}{\partial y}\right) + \frac{\partial}{\partial y}\left(\mu_t \frac{\partial \bar{v}}{\partial y}\right)$$

From Figure 7, the $\overline{v'^2}$ is asymmetric for the smaller and the largest swirl numbers. As these fluctuations are perpendicular to the axial flow direction, they are linked to the flow flapping effects and may be the cause of asymmetrical flows as a result of non-axisymmetric swirl generation. At the intermediate swirl number, the $\overline{v'^2}$ is asymmetric inside the burner outer diameter. This can again be the reason for the asymmetrical flow; although more symmetrical than the other two swirl numbers.

Values of $\overline{u'v'}$ presented in Fig. 9 are generally smaller than that of $\overline{u'^2}$ (Fig. 6) and $\overline{v'^2}$ (Fig. 7). The values of $\overline{u'v'}$ range from ±3 m^2/s^2 (S=0.3) to ±5 m^2/s^2 (S=1.07). Non-zero fluctuations are observed for all axial locations and over all radial locations.

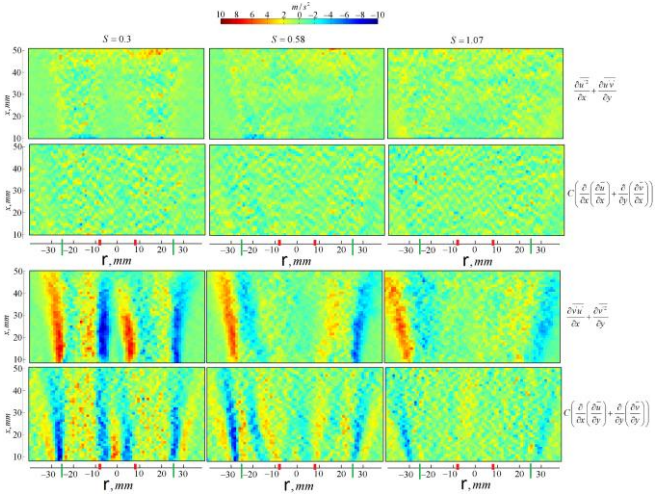

Figure 9: Spatial distribution of additional source terms in u-momentum equation $\partial\overline{u'^2}/\partial x + \partial\overline{u'v'}/\partial y$, spatial distribution of additional source terms in v-momentum equation $\partial\overline{v'u'}/\partial x + \partial\overline{v'^2}/\partial y$ and application of the Boussinesq approximation for incompressible flows for corresponding u, v-momentum equations as a function of flow swirl number. Note that Boussinesq approximation for u and v momentum equation was multiplied with an experimentally found constant of C=15.

The maximum and minimum values of the additional source term in the u-momentum equation are between 0-2 m/s^2. They are almost uniformly distributed and are independent of the flow swirl number (top row in Fig. 9). The spatial distributions of the additional source term of the v-momentum equation were found to be highly non-uniform and fluctuated between ±10 m/s^2. The maximum and minimum values are found within regions of high shear stress, i.e. at the shear layer between the non-swirling jet and the swirling co-flow and the swirling co-flow and the ambient air. Therefore, it was found that the additional source term in the u-momentum equation is about 20% of the same in the v-momentum equation. Comparing the raw experimental values and the mean velocity based gradient values, suggests an 'effective' turbulent viscosity of 15 m^2/s.

It is known that a turbulence model must satisfy the Schwarz inequality. Once this inequality is satisfied, the normal Reynolds stresses are always non-negative and the variance of any scalar fluctuations is always positive. Therefore, the concept of realisability was introduced to turbulence modelling to ensure that turbulence models do not produce non-physical results (Schumann, 1977; Charles *et al.*, 1994). Lumley (1979) formulated the principles of realisability by analysing the eigenvalues of the turbulent correlation matrix, which is written as.

$$\begin{pmatrix} \overline{u'^2} & \overline{u'v'} \\ \overline{u'v'} & \overline{v'^2} \end{pmatrix} \quad (6)$$

The eigenvalues of the turbulent correlation matrix can be computed as (Hallback et al., 1995).

$$\lambda_{1,2} = 0.5\left\{\left(\overline{u'^2}+\overline{v'^2}\right) \pm \sqrt{\left(\overline{u'^2}+\overline{v'^2}\right)^2 - 4\left(\left(\overline{u'^2}\cdot\overline{v'^2}\right)-\left(\overline{u'v'}\right)^2\right)}\right\} \quad (7)$$

It can be shown that if the eigenvalues of the turbulent correlation matrix written above are always non-negative, the following inequalities are satisfied (Hallback et al., 1995).

$$\begin{aligned} &\overline{u'^2} \geq 0, \overline{v'^2} \geq 0 \\ &\overline{u'^2}\cdot\overline{v'^2} - \overline{u'v'}^2 \geq 0 \end{aligned} \quad (8)$$

Figure 10 shows the Schwarz inequality computed from last expression of Eq. 8 for the flow swirl numbers studied in this article. This quantity is indeed always positive. The values of Schwarz inequality were found to be within 600-800 m^4/s^4 for flow swirl number of 0.3-0.58 and 600-1200 m^4/s^4 for S=1.07. The spatial distributions of the Schwarz inequality are similar to the spatial distributions of the standard deviations of velocity fluctuations, which were shown in Figure 4 and are nearly axisymmetric for *S*=0.3 and 1.07 but slightly distorted for *S*=0.58.

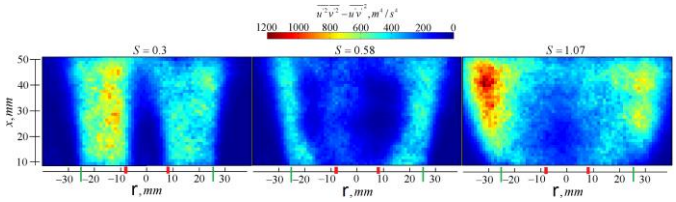

Figure 10: Schwarz inequality as a function of flow swirl number. From left to right *S*=0.3, 0.58 and 1.07.

4 Conclusions

Coaxial swirling jets with low, intermediate and high swirl numbers were experimentally studied by considering the spatial distributions of velocity, vorticity, velocity fluctuations and the Reynolds stresses. The swirling flows were formed by discharging a central jet of air in an annular stream of swirling air flow. This is a typical geometry used in swirl-stabilised burners, where the central jet is the fuel. The behaviours of the unclosed terms $\overline{u'^2}$, $\overline{v'^2}$, $\overline{u'v'}$, and their gradients, which appear in the RANS equations were analysed as a function of the swirl number. The values of the Schwarz inequality $\overline{u'^2}\cdot\overline{v'^2} - \overline{u'v'}^2$ were presented.

The results showed pronounced asymmetry in the mean and the fluctuating quantities for all swirl numbers, which may be linked to not axisymmetric swirl generation. It is postulated that any swirl generator that is based on, e.g. tangential injection with milled slots or nozzles as well as passive vanes results in phase-dependent variations in the ensemble mean velocities and the Reynolds stresses. Modelling of swirling flames or jets, which are generated by passive vanes (static swirlers), e.g. in GT combustors, as axisymmetric jets may not always be plausible due to inherent asymmetry. The ratio of $\overline{u'^2}/\overline{v'^2}$ was found to be circa 0.5 and was independent of the flow swirl number. The values of $\overline{u'v'}$ were circa 5-10% of $\overline{v'^2}$. It was postulated that for constant Reynolds number, change in the flow swirl number did not necessary result in increase of turbulent intensity.

The relative contributions of the additional source terms in the *u*-momentum conservation equation, corresponding to velocity fluctuations along the jet axis, to the overall Reynolds stress was found to be within 20%. Comparing the raw experimental values and the mean velocity based gradient values, suggested an 'effective' turbulent viscosity of 15 m2/s.

5 Acknowledgement

The work was supported in part by the Alan Howard scholarship for Energy Futures to the first author.

6 Nomenclature

S – is the flow swirl number
G_θ – is the axial flux of angular momentum
G_x – is the axial flux of axial momentum
ρ – is the density
U,V,W – are the ensemble-averaged components of velocity
r_i – is the radius of the inner pipe
$\overline{u'^2}, \overline{v'^2}, \overline{w'^2}$ – are the normal Reynolds stress terms
σ_V – is the standard deviation of velocity fluctuations
N – is the number of PIV instantaneous images
V – is the velocity magnitude
μ_t – is the turbulent viscosity

References

Lilley, D.G. (1977) 'Swirl flows in combustion: a review', *AIAA Journal*, Vol. 15, No. 8, pp.1063-1078.

Hoekstra, A.J., Derksen J.J. and Van Den Akker, H.E.A. (1999) 'An experimental and numerical study of turbulent swirling flow in gas cyclones', *Chem. Eng. Sci.*, No. 54, pp.2055-2065.

Ribeiro, M.M, and Whitelaw, J.H., (1980) 'Coaxial jets with and without swirl', *J. Fluid Mech*. Vol. 96, No. 4, pp.769-795.

Farokhi, S., Taghavi, R. and Rice, E.J. (1992) 'Modern developments in shear flow control with swirl', AIAA Journal, Vol. 30, No. 6, 30, 1482-1483.

Gupta, A.K., Lilley, D.G. and Syred, N. 'Swirl flows,' ABACUS Press, Cambridge, USA, 1985.

Syred, N. and Beer, J.M. (1974) 'Combustion in swirling flows: a review', *Combust. Flame*, Vol. 23., No. 2, pp.143-201.

Gupta, A., Mehta, R.S., Wang, A., Haworth, D.C. and Modest, M.F. 'A LES/FDF/PMC model for luminous turbulent flames.' In: Proceedings of the sixth joint meeting of the U.S. sections of the combust. institute, Ann Arbor, MI 17-20 May 2009.

Rose, W.G. (1962) 'A swirling turbulent round jet', *J. Appl. Mech*. Vol. 29, No. 4, pp.615-625.

Craya, A. and Darrigol, M. (1967) 'Turbulent swirling jet', *Phys. Fluids Suppl*. Vol. 10, No. 9, pp.S197-S199.

Chigier, N.A. and Chervinsky, A. (1967) 'Experimental investigation of swirling vortex motions in jets', *J. Appl. Mech*., Vol. 34, No. 2, pp.443-451.

Kawaguchi, O. and Sato, G.T. (1971) 'Experimental investigation of premixed swirling jet flames (velocity and turbulence intensity of swirling air jets)', *Bull. J.S.M.E*. Vol. 14, pp.248-256.

Chigier, N.A. and Beer, J.M. (1964) 'The flow region near the nozzle in double concentric jets', Trans. A.S.M.E.D, *J. Basic Engng*. Vol. 86, No. 4, pp.797-804.

Huang, R.F., Duc, L.M. and Hsu, C.M. (2016) 'Flow and mixing characteristics of swirling double-concentric jets influenced by a control disc at low central jet Reynolds numbers', *Int. J. Heat Fluid Flow*, Vol. 62, Part B, 233-246.

Stetsyuk, V., 'Experimental study of combustion and scalar mixing in swirling jet flows', PhD thesis (Imperial College London, Department of Mechanical Engineering. February 2014).

Facciolo, L., 'A study on axially rotating pipe and swirling jet flows', PhD thesis, (KTH Mechanics, Stockholm, Sweden, TRITA-MEK Tech. Rep. 2006:02, 2006).

Orlu R., Experimental study of passive scalar mixing in swirling jet flows, PhD thesis (Technical Reports from Royal Institute of Technology KTH Mechanics, Stockholm, Sweden. September 2006).

Toh, I.K., Honnery, D. and Soria J., 'Velocity and scalar measurements of a low swirl jet,' In Proc. 4th Australian Conf. Laser Diagnostics Fluid Mech. Comb., 129-132, The University of Adelaide, South Australia, Australia, 2005.

Gilchrist, R.T. and Naughton, J.W. (2005) 'An experimental study of incompressible jets with different initial swirl distributions: Mean results', *AIAA J*. Vol. 43, No. 4, 741-751.

Oljaca, M., Gu, X., Glezer, A., Baffico, M. and Lund F. (1998) 'Ultrasound scattering by a swirling jet', *Phys. Fluids*, Vol. 10, No. 4, pp.886-898.

Feyedelem, M.S. and Sarpkaya, T. (1998) 'Free and near free surface swirling turbulent jets', AIAA J. Vol. 36, No. 3, pp.359-364.

Park, S.H. and Shin, H.D. (1993) 'Measurements of entrainment characteristics of swirling jets', *Int. J. Heat Mass Transfer*, Vol. 36, No. 16, pp.4009-4018.

Milosavljevic, V.D., Natural gas, kerosene and pulverized fuel fired swirl burners, PhD thesis (Imperial College of Science Technology and Medicine. Department of Mechanical Engineering. 1993).

Mehta, R.D., Wood, D.H. and Clausen, P.D. (1991) 'Some effects of swirl on turbulent mixing layer development', *Phys. Fluids*, Vol. 3, No. 11, pp.2716-2724.

Farokhi, S., Taghavi, R. and Rice, E.J. (1989) 'Effect of initial swirl distribution on the evolution of a turbulent jet', *AIAA J.*, Vol. 27, No. 6, pp.700-706.

Elsner, J.W. and Kurzak, L. (1989) Semi-preserving development of a slightly heated free swirling jet', *J. Fluid Mech*., Vol. 199, pp.237-255.

Samet, M. and Einav, S. (1988) 'Mean value measurements of a turbulent swirling-jet', *AIAA J*., Vol. 26, No. 5, pp. 619-621.

Liang, H. and Maxworthy, T. (2005) 'An experimental investigation of swirling jets,' *J. Fluid Mech*., Vol. 525, No. pp.115-159.

Kito, O. (1984) 'Axi-asymmetric character of turbulent swirling flow in a straight circular pipe', *Bulletin of JSME*, Vol. 27, pp.683-690.

Panda, J. and McLaughlin, D.K. (1994) 'Experiments on the Instabilities of a swirling jet', *Phys. Fluids*, Vol. 6, No. 1, pp.263-276.

Steenbergen, W. Turbulent pipe ow with swirl, PhD thesis (Technishe Universiteit Eindhoven, Netherlands. 1995).

Stetsyuk V., Soulopoulos, N., Hardalupas, Y. and Taylor, A.M.K.P. (2016) Scalar dissipation rate statistics in turbulent swirling jets', *Phys. Fluids*, Vol. 28, No. 7, pp.075-104.

Stanislas, M., Okamoto, M., Kahler, C.J. and. Westerweel, J. (2005) 'Main results of the second international PIV challenge,' *Exp. Fluids*, Vol. 39, No. 2, 170-191.

Melling, A. (1997) ‘Tracer particles and seeding for particle image velocimetry’, *Meas. Sci. Technol*. Vol., 8, No. 12, pp.1406-1416.

Tropea, C. Yarin, A. and Foss J.F. (Eds.), Springer Handbook of Experimental Fluid Mechanics," Springer Verlag Berlin, Heidelberg, 2007.

Panton, R.L. ‘Vorticity Dynamics, in Incompressible Flow, Fourth Edition’, John Wiley & Sons, Inc., Hoboken, NJ, USA, 2013.

Clayton, B.R. and Morsi, Y.S.M. (1985) Determination of principal characteristics of turbulent swirling flow along annuli. Part 2: Measurement of turbulence components’, Int. *J. Heat & Fluid Flow*, Vol. 6, No. 1, pp.31-41.

Schumann, U. (1977) ‘Realizability of Reynolds stress turbulence models’, *Phys. Fluid*, Vol. 20, No. 5, pp.721-725.

Speziale, C.G., Abid, R. and Durbin, P.A. (1994) ‘On the realizability of Reynolds stress turbulence closures, *J. Scientific Computing*, Vol. 9, No. 9, pp.369-403.

Lumley, J.L. (1979) ‘Computational modeling of turbulent flows’, *Adv. Appl. Mech.*, Vol. 18, No., pp.123-176.

Hallback, M., Henningson, D.S., Johansson, A.V. and Alfredsson, P.H. Turbulence and Transition Modelling (Springer Netherlands, 1995).